

# Spectroscopy and dissociative recombination of the lowest rotational states of $H_3^+$

A Petrigani<sup>1</sup>, H Kreckel<sup>2</sup>, M H Berg<sup>1</sup>, S Altevogt<sup>1</sup>, D Bing<sup>1</sup>,  
H Buhr<sup>3</sup>, M Froese<sup>1</sup>, J Hoffmann<sup>1</sup>, B Jordon-Thaden<sup>1</sup>, C Krantz<sup>1</sup>,  
M B Mendes<sup>1</sup>, O Novotný<sup>1</sup>, S Novotny<sup>1</sup>, D A Orlov<sup>1</sup>, S Reinhardt<sup>1,4</sup>,  
and A Wolf<sup>1</sup>

<sup>1</sup> Max-Planck-Institut für Kernphysik, Saupfercheckweg 1, D-69117 Heidelberg, Germany

<sup>2</sup> Columbia University, 550 West 120th Street, New York, NY 10027, USA

<sup>3</sup> Department of Particle Physics, Weizmann Institute of Science, 76100 Rehovot, Israel

E-mail: Annemieke.Petrigani@mpi-hd.mpg.de

**Abstract.** The dissociative recombination of the lowest rotational states of  $H_3^+$  has been investigated at the storage ring TSR using a cryogenic 22-pole radiofrequency ion trap as injector. The  $H_3^+$  was cooled with buffer gas at  $\sim 15$  K to the lowest rotational levels,  $(J, G)=(1,0)$  and  $(1,1)$ , which belong to the ortho and para proton-spin symmetry, respectively. The rate coefficients and dissociation dynamics of  $H_3^+(J, G)$  populations produced with normal- and para- $H_2$  were measured and compared to the rate and dynamics of a hot  $H_3^+$  beam from a Penning source. The production of cold  $H_3^+$  rotational populations was separately studied by rovibrational laser spectroscopy using chemical probing with argon around 55 K. First results indicate a  $\sim 20\%$  relative increase of the para contribution when using para- $H_2$  as parent gas. The  $H_3^+$  rate coefficient observed for the para- $H_2$  source gas, however, is quite similar to the  $H_3^+$  rate for the normal- $H_2$  source gas. The recombination dynamics confirm that for both source gases, only small populations of rotationally excited levels are present. The distribution of 3-body fragmentation geometries displays a broad part of various triangular shapes with an enhancement of  $\sim 12\%$  for events with symmetric near-linear configurations. No large dependences on internal state or collision energy are found.

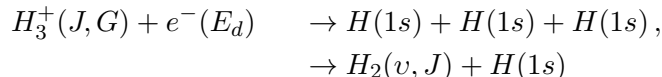
## 1. Introduction

The  $H_3^+$  ion is of utmost theoretical and astrophysical importance. It is the simplest polyatomic ion and thereby constitutes an important benchmark ion for the theory of both molecular structure and molecular collision dynamics. It is also a key ion in the universe as it initiates a network of reactions leading to the formation of complex molecules. The dissociative recombination (DR) of  $H_3^+$  plays a crucial role as destruction mechanism for the  $H_3^+$  ions [1, 2] and as production mechanism for the neutral hydrogen fragments. The DR reaction has been extensively researched over the past decades [3, 4] and with the knowledge on the reaction increasing, the focus is moving to more and more detailed investigations. Internal-state dependences of the DR reaction, at zero as well as at elevated electron energies, are now being studied [5, 6]. Disagreements on the magnitude of the DR rate coefficient of  $H_3^+$  have been dominating the scene for quite some time [7]. Presently, the differences that have been observed

<sup>4</sup> Present address: Max-Planck-Institut für Quantenoptik, Garching, Germany

are attributed to different internal-state distributions of the ions and consent between storage-ring experiments has been reached [8, 9]. Furthermore, previous discrepancies with afterglow studies seem to have been resolved recently and the latest theoretical calculations show good overall agreement with experiment [10, 11, 12]. However, the predicted rate coefficient still shows local discrepancies up to an order of magnitude around several electron energy regions. Again, differing internal-state distributions are given as possible explanation. In the cold interstellar space, the difference of the DR rate between the two lowest rotational levels,  $(J, G)=(1,0)$  and  $(1,1)$  at an energy difference corresponding to  $kT=33$  K only, may be of particular importance. Since for  $H_3^+$  these two levels are equivalent with the ortho and the para symmetry of the total nuclear spin, respectively, we shortly denote the two levels as ortho- and para- $H_3^+$ . Previous experiments indicate that the DR rate coefficient of para- $H_3^+$  could be larger than that of ortho- $H_3^+$  for specifically the low electron energies prevailing in the cold interstellar medium [9]. In these experiments, para- $H_2$  was used as precursor gas and although the rotational populations of the  $H_3^+$  ion beam could not be measured, an enhancement of the para- $H_3^+$  population is expected in this case. The higher para- $H_3^+$  rate was until recently in contradiction to theory, which predicted the opposite [11, 13]. However, new theoretical results now state a roughly ten times higher rate for para- $H_3^+$  at low temperature [12].

The DR of cold  $H_3^+$  has two fragmentation channels for low-energy electrons, a 3-body breakup containing only ground-state atoms and a 2-body breakup that includes the  $H_2$  product molecule,



Here, the cold initial  $H_3^+$  ion is given to be in a low rotational state of its ground vibrational state with  $J$  the total angular momentum associated with the motion of the nuclei and  $G = |K - l|$ , where  $K$  is the projection of  $J$  onto the molecular axis and  $l$  is the vibrational angular momentum. The product atoms are in their ground state, whereas the  $H_2$  molecule may be rovibrationally,  $(v, J)$ , excited. Further dissociation channels become possible when additional energy,  $E_d$ , is introduced via the electrons. At typical molecular-cloud temperatures of 10-60 K,  $H_3^+$  populates the two to three lowest rotational levels,  $(J, G)=(1,0)$ ,  $(1,1)$ , and  $(2,2)$ , of the vibrational ground state, where the  $(2,2)$  level belongs to the para spin symmetry.

We present a two-fold investigation of cold  $H_3^+$ . The first focus is on the production and characterisation of rotationally cold  $H_3^+$  populations using normal- $H_2$  and para- $H_2$  as parent gas. In order to probe the different rotational distributions, rovibrational spectroscopy on the  $H_3^+$  ions in a 22-pole radiofrequency ion trap is implemented. The second focus is on the DR of  $H_3^+(J, G)$  populations with altered ortho-to-para ratio. High-resolution rate coefficients up to 0.4 eV are given and additionally compared to a hot  $H_3^+$  beam to investigate rotational heating. The issue of internal excitation is addressed by fragment imaging. For the first time, the dissociation of  $H_3^+$  were studied using the 3D imaging technique [14], and 3-body breakup from both 2D and 3D imaging are presented.

## 2. Experimental Setup

The cold  $H_3^+$  samples are prepared in a 22-pole radiofrequency (rf) ion trap setup, as shown in the inset of Figure 1. The ions are produced in a rf storage ion source [15] through electron-impact ionisation of  $H_2$  and subsequent collisions of the  $H_2$  with the hence produced  $H_2^+$ . The  $H_3^+$  ions are then guided through a rf quadrupole to the 22-pole rf ion trap [16]. Here, the ions are trapped radially by the 22 poles and axially by an entrance and exit electrode. The number of stored ions may be varied from a few to several millions of ions, whereas the storage time may be varied from ms to several seconds. During storage, the ions are buffer-gas cooled with helium

at a chosen ambient temperature of 10-60 K. For more details on the 22-pole trap setup, the reader is referred to Refs. [17, 18]. In the present work, the setup is used as a stand-alone device for probing the  $H_3^+(J, G)$  populations implementing rovibrational spectroscopy and it is used as an ion injector for the storage ring TSR to the study of the DR of the cold  $H_3^+$  (see Figure 1). Unfortunately, the conditions required for the spectroscopy measurements are different from those of the DR measurements. As such, care has to be taken when deploying information from the laser-probed populations for the TSR measurements.

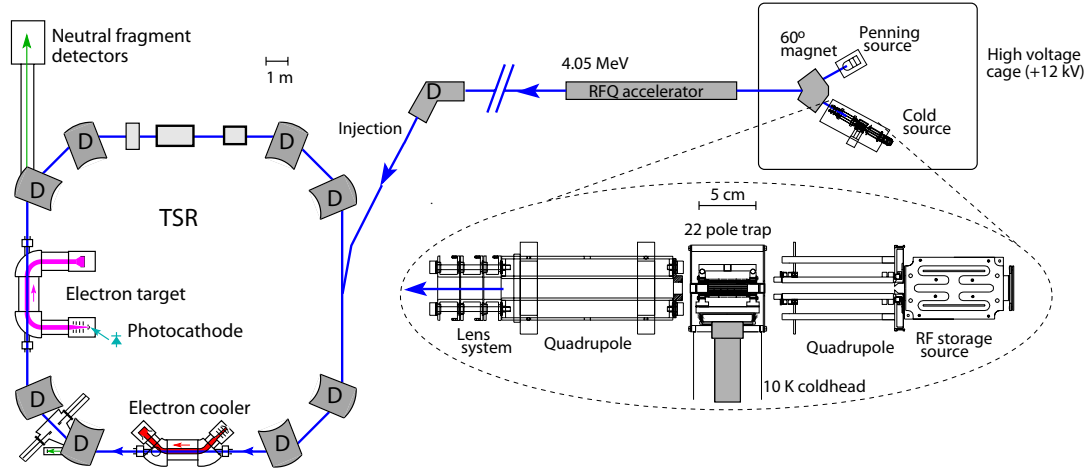
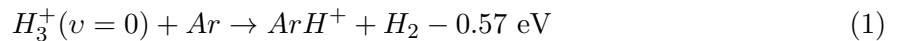


**Figure 1.** The 22-pole trap setup used as injector for the ion storage ring TSR. The  $H_3^+$  ions are prepared in the trap, accelerated to 4.05 MeV, and injected into the ring. A cold electron beam, produced with a liquid-nitrogen cooled photocathode [19], is merged with the ion beam in the electron target. The neutral fragments are detected either with a surface barrier counting detector or a position-sensitive imaging system [20, 21].

### 2.1. Spectroscopy Experiments

To verify the buffer-gas cooling inside the 22-pole trap and to probe the rotational-state populations, an action spectroscopy scheme is used. To this purpose, rovibrational spectroscopy in the infrared is implemented as  $H_3^+$  lacks any stable electronically excited states. As a sensitive probe of the vibrational transitions, a laser-induced chemical reaction with argon as reactant is used. The charge exchange reaction,



is endothermic by 0.57 eV for ground-state  $H_3^+$  ions. However, if at least two vibrational quanta are excited in  $H_3^+$ , the reaction becomes energetically possible. Once the ions in the trap are cooled down to the chosen temperature, a tunable infrared diode laser of  $\sim 1400$  nm is used to trigger transitions from the lowest rotational states of  $H_3^+$  to the third harmonic of the bending-mode vibration. The laser-excited ions will react with the abundant argon in the trap to form  $ArH^+$ , which is trapped as well and used as spectroscopic signal. The ions are extracted from the trap, analysed by a mass spectrometer, and directed to a scintillation detection system capable of counting single ions with near-unity efficiency. These spectroscopy measurements are performed at a minimum temperature of 55 K to keep the argon in the gas phase. For more details, see Ref. [17].

The action spectroscopy scheme has been used before to probe cold  $H_3^+$  produced with normal- $H_2$  [17]. Here, also the  $H_3^+$  rotational distribution produced with para- $H_2$  is presented.

Moreover, important improvements have currently been implemented to enhance the cooling of the  $H_3^+$  in the trap as well as to enhance the  $ArH^+$  spectroscopy signal. Gas purities, laser power (increased by a factor of 10), and frequency resolution have now been refined. As a result, the typical  $ArH^+$  count at resonance is 1.5-2 per trap filling of 300  $H_3^+$  ions, an order of magnitude higher than before. The number densities of the helium and argon gas inside the trap have been optimised to  $\sim 10^{14}$   $\text{cm}^{-3}$  and  $\sim 10^{12}$   $\text{cm}^{-3}$ , respectively. The hydrogen number density,  $\sim 10^{10}$   $\text{cm}^{-3}$ , and the trap storage time, 250 ms, were unchanged.

## 2.2. Dissociative Recombination Experiments

The DR measurements were performed with the 22-pole trap as injector of the cold ion beam for the storage ring TSR. The trap temperature was set to 15 K in order to simplify the DR measurements, as only the lowest para and ortho rotational states, (1,0) and (1,1), are populated at that temperature. The number of  $H_3^+$  ions had to be hugely increased to the maximum trap filling of around  $2 \cdot 10^6$  in order to supply a sufficient DR count rate [22]. The  $H_3^+$  ortho-to-para ratio is dominantly determined by collisions with  $H_2$ , therefore the  $H_2$  number density ( $10^{10}$   $\text{cm}^{-3}$ ) was kept the same as in the spectroscopy experiments. The helium number density was increased to  $\sim 10^{15}$   $\text{cm}^{-3}$  to compensate for the slightly reduced trap storage time of 100 ms. After this cooling time, the ions were released to be accelerated and stored in the TSR at an ion-beam energy of 4.05 MeV. The transmission of the ion beam was about 10%, resulting in very low counting rates (in a later storage-ring experiment the transmission could be improved to 50%). The ring storage time was set to 10 s during which the ion beam was merged in the electron target with an ultracold electron beam produced by a liquid-nitrogen cooled photocathode [19]. The transversal and longitudinal temperatures of this electron beam were  $T_{\perp} = 1$  meV and  $T_{\parallel} = 30$   $\mu\text{eV}$ , respectively. The electron density was roughly  $9 \cdot 10^5$   $\text{cm}^{-3}$ . Rate-coefficient curves were measured with a new large surface barrier detector of  $10 \times 10$   $\text{cm}^2$  at collision energies between 0 and 0.4 eV by varying the electron detuning energy,  $E_d$ . The dynamics of the DR reactions were investigated at  $E_d = 0$  and 6 meV through the  $2D$  [20] and, as a first for  $H_3^+$ , the  $3D$  [14, 21] imaging technique. The electron cooler was set to 0 eV collision energy to continuously cool the ion beam and, for the first 0.5 s of storage, the electron target was additionally set to 0 eV in order to speed up the initial translational phase-space cooling of the beam. This initial cooling time was deliberately kept low in order to minimise possible internal heating-effects from the toroidal regions, where the electron beam is no longer parallel to the ion beam and elevated detuning energies may cause rotational excitation of the ions. Only for the 0-eV imaging measurements, the electron cooler was switched off after this time, whilst the target remained at 0 eV.

## 3. Results

### 3.1. Rovibrational Spectroscopy

Figure 2 shows the observed  $ArH^+$  signal for the transitions from the three lowest rotational states present at 55 K to the third vibrational level. The upper figure results from  $H_3^+$  ions produced with normal- $H_2$ , the lower from  $H_3^+$  ions produced with para- $H_2$ . We are currently still studying possible effects of the change of the precursor gas on the absolute normalisation of the signal. The relative normalised intensities for a given normal- $H_2$  or para- $H_2$  measurement, however, are reproducible and well under control. The intensities are normalised to the laser power of  $\sim 12$  mW, to a trap filling of 300 ions, and to an  $ArH^+$  lifetime of 25 ms, such that they may be coarsely compared to the previously published spectroscopy measurement [17].

The experimental changes mentioned before have now lead to improved signal strengths giving rise to nicely observable Gaussian profiles. The cooling of the ions also proved to be more efficient at the optimised helium pressure and much lower temperatures are observed than in 2004 [17]. The profile widths of the respective transitions denoted by  $R(J,G)$  – where  $R$

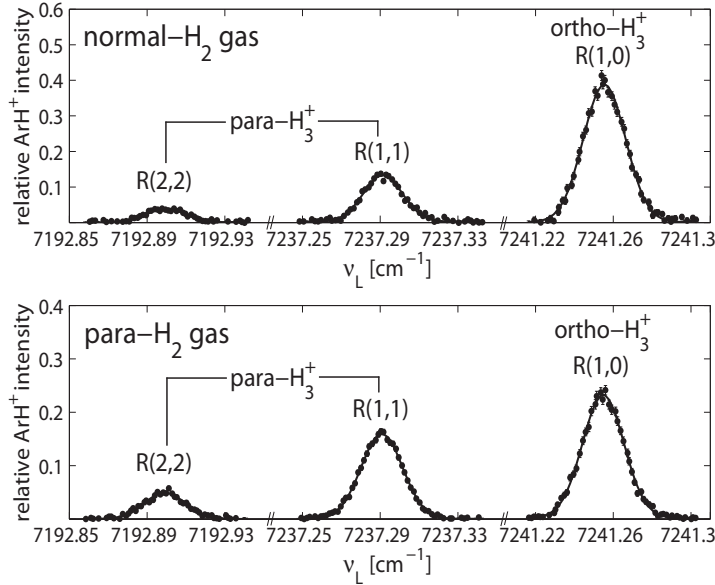


**Figure 2.** The measured absorption profiles for the three observed transitions in the  $(0, 3^1) \leftarrow (0, 0^0)$  vibrational overtone band of  $H_3^+$  produced with normal- $H_2$  (upper panel) and para- $H_2$  (lower panel). The signal is derived by averaging over many trap fillings.

stands for the  $(J+1)$  branch and  $J, G$  stand for the rotational quantum numbers of the lower state – are determined by Doppler broadening, which conforms a temperature of  $\sim 67$  K for all transitions. The line-intensity ratios are determined by the given laser intensity, the Einstein coefficients, and the initial-level populations. Assuming the theoretical Einstein coefficients of  $8.9$ ,  $4.9$ , and  $8.2 \text{ s}^{-1}$  for  $R(1, 0)$ ,  $R(1, 1)$ , and  $R(2, 2)$ , respectively [23], the populations and hence ortho-to-para and para-to-para ratios can be extracted. The “para rotational temperature” is derived from the ratio between the two para transitions,  $R(1, 1)$  and  $R(2, 2)$ , and matches the translational temperature of  $\sim 67$  K for both ion-source gases. Thermal equilibrium seems to have been reached in both cases. The “ortho-to-para temperature” is derived from the ratio between the ortho transition,  $R(1, 0)$ , and the para transitions,  $R(1, 1) + R(2, 2)$ . A significant decrease of the ortho- $H_3^+$  line relative to the para lines is visible when using para- $H_2$  as parent gas. The ortho-to-para temperature correspondingly decreases, namely from  $\sim 140$  K to  $\sim 36$  K. This clearly shows that under certain circumstances the ortho-to-para ratio can become non-thermal and can deviate significantly from the translational and rotational temperature of an ion sample. The population for the normal- $H_2$  parent gas conforms an ortho-to-para ratio of 60:40 using the above mentioned Einstein coefficients, whereas the  $H_3^+$  sample produced with para- $H_2$  shows the opposite, an ortho-to-para ratio of 40:60. It seems that the use of para- $H_2$  as parent gas leads to enrichment of the rotational states belonging to the para- $H_3^+$  symmetry.

### 3.2. Dissociative Recombination Rate Coefficients

As mentioned before, the 22-pole trap was used as an injector for the storage ring TSR, where the DR rate of the cold  $H_3^+$  populations was investigated between 0 and 0.4 eV collision energy. Also, to investigate rotational heating, the DR rate of a hot  $H_3^+$  beam produced with a Penning source was measured. Due to low count rates for the cold ion beams (only 10% transmission), insufficient statistics could be gathered around the 10-eV resonance. Therefore, the rate curves have been normalised to the 12-meV resonance. This resonance is at an energy low enough for sufficient statistics, however, presumably at an energy high enough for the normal- and para- $H_3^+$  rates to be the same, as observed in Ref. [9]. The hot  $H_3^+$  rate curve, which does contain enough statistics, is normalised to the 10-eV resonance. Both normalisations are to the photocathode measurement of Ref. [9] as it bears a similar energy resolution. Figures 3 and 4 show the reduced rate coefficients,  $\alpha \cdot \sqrt{E_d}$ , with  $\alpha$  the energy-dependent rate coefficient that is proportional to

$\sqrt{E_d}$ . Any structures observable on the reduced rate are related to resonant behaviour. Figure 3 (upper frame) displays the measured rates of the hot and cold  $H_3^+$  produced with normal- $H_2$ . Overall, the hot  $H_3^+$  rate is higher than the cold  $H_3^+$  rate, except for the resonance around 7 and 270 meV. Although the temperature of the  $H_3^+$  beam from the Penning source is on the order of  $10^3$  K (see Section 3.3), resonant behaviour is still clearly visible. Figure 3 (lower frame) shows the theoretical predictions for 100 K and 1000 K as calculated by Ref. [12]. Similar to the experiment, the hot  $H_3^+$  rate is overall higher, however, at very low energies, the opposite behaviour is predicted. Several structures appear both in theory and in experiment. The intensities of the theoretical rates seem to be systematically lower than those measured, leading to a better agreement between our cold  $H_3^+$  beam and the 1000 K theoretical rate. This raises the question whether heating effects in the storage ring might have considerably warmed up the initially cold ion beam. The fragmentation dynamics presented in the next section, however, demonstrate that this is not the case.

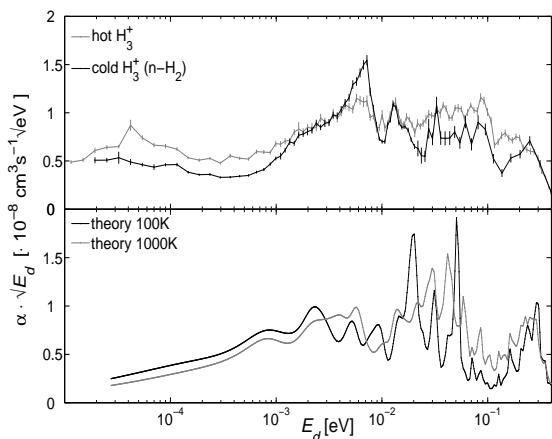


**Figure 3.** The upper frame shows the measured reduced rate coefficients of the cold (black) and hot (grey)  $H_3^+$  produced with normal- $H_2$  in the 22-pole trap and the Penning source, respectively. The lower frame shows the reduced theoretical rates for 100 K (black) and 1000 K (grey), folded with the experimental electron temperature from Ref. [12].

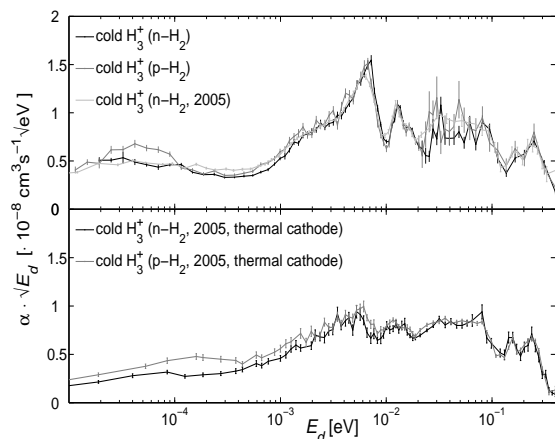


**Figure 4.** The upper frame shows the high-resolution reduced rates of  $H_3^+$  produced with para- $H_2$ , present data (grey), and normal- $H_2$ , present data (black) and previous data (light grey) [9]. The lower frame shows the previously measured lower-resolution reduced rates of  $H_3^+$  produced with para- $H_2$  (grey) and normal- $H_2$  (black) [9].

Figure 4 displays the reduced rates of the cold  $H_3^+$  ion beams produced with normal- and para- $H_2$  (upper frame). The  $H_3^+$  rate using para- $H_2$  exhibits slightly more structure below 5 meV collision energies. Otherwise, the rate coefficients are quite similar and show no sign of the predicted order of magnitude difference in DR rate between para- $H_3^+$  and ortho- $H_3^+$  [12]. The two  $H_3^+$  populations in the storage ring produced with normal- and para- $H_2$  are unknown and may very well differ less than was the case in the spectroscopy measurements, however, a DR rate that is an order of magnitude faster for para- $H_3^+$  than for ortho- $H_3^+$  should manifest itself even at small increases in the para- $H_3^+$  contribution. No large dissimilarities between the two source gases are observed that would point towards the predicted ten times more rapid dissociation of para- $H_3^+$ . Still, nearly identical  $H_3^+(J, G)$  populations in the storage ring for both source gases cannot be excluded.

Also shown in figure 4 is the previous photocathode measurement for normal- $H_3^+$  (upper

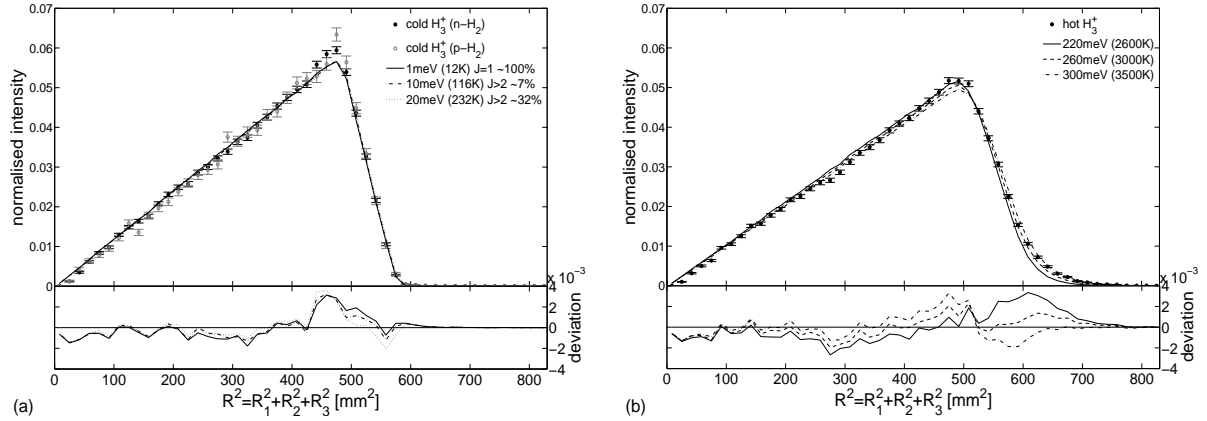


**Figure 5.** The  $R^2$  distributions of the  $H_3^+$  beams for (a) the cold  $H_3^+$  produced with normal- and para- $H_2$  in the 22-pole trap and (b) the hot  $H_3^+$  produced with normal- $H_2$  in the Penning source. All black curves are Monte-Carlo simulations of isotropic dissociations at the given temperatures, considering the allowed rotational levels and their probability in a Boltzmann distribution. All distributions are normalised to unit area. The deviation of the measured distributions of  $H_3^+$  produced with normal- $H_2$  from the simulations are plotted in the respective lower frames.

frame) and the previously measured  $H_3^+$  rates for the normal- and para- $H_2$  source gases as measured with the thermal cathode (lower frame) [9]. The photocathode data clearly exhibit more pronounced resonances as the resolution of the liquid-nitrogen cooled photocathode ( $T_{e,\perp} = 1$  meV) [19] is much better than that of the thermal cathode ( $T_{e,\perp} = 4$  meV). A small resonance is revealed around 17 meV and below 5 meV structure is unfolded. The increased structure visible for the para- $H_2$  source gas raises the  $H_3^+$  rate slightly, in accordance with the previous thermal-cathode experiment, i.e., assuming the normalisation on the 12-meV resonance is valid. Further analysis is still required. It is noted that the internal distributions in the ring may also differ between the present and previous DR experiments, both in ortho-to-para ratio for the  $H_3^+$  produced with para- $H_2$  as in the achieved internal temperature that may give rise to a differing contribution from excited rotational levels irrespective of source gas.

### 3.3. Dissociative Recombination Dynamics

The breakup dynamics of the DR of  $H_3^+$  and their possible  $(J, G)$  state-dependences have been studied as well. Imaging data have been taken for both the 2-body and 3-body fragmentation channel. Here, only dissociation into three  $H$  atoms is treated. Figure 5a) shows the projected distance distributions of our cold  $H_3^+$  beams from the 22-pole trap as acquired by the 2D imaging [20], normalised to unit area. The distance plotted is  $R^2 = R_1^2 + R_2^2 + R_3^2$  with  $R_i$  the distance from particle  $i$  to the centre-of-mass in the 2D detection plane. Forward Monte-Carlo simulations for isotropic dissociations at three different rotational temperatures, normalised to unit area, are plotted to reveal a rough estimate of the temperature of the ion beam and anisotropy effects. To clarify differences, the deviation of the distribution for the normal- $H_2$  source gas from the simulations is displayed in the lower frame. The discrepancy at the peak of the distribution could indicate anisotropy and further simulations are needed to investigate the observed feature. Figure 5b) shows the  $R^2$  distribution of the hot  $H_3^+$  from the Penning source together with forward simulations at three high temperatures. Below, the difference of the measured data with the simulations is shown. Again, no large anisotropies can be observed.

The best temperature fit is determined from the least-squares minimum between the falling slope of the data and the simulation, with the simulation normalised to the maximum of

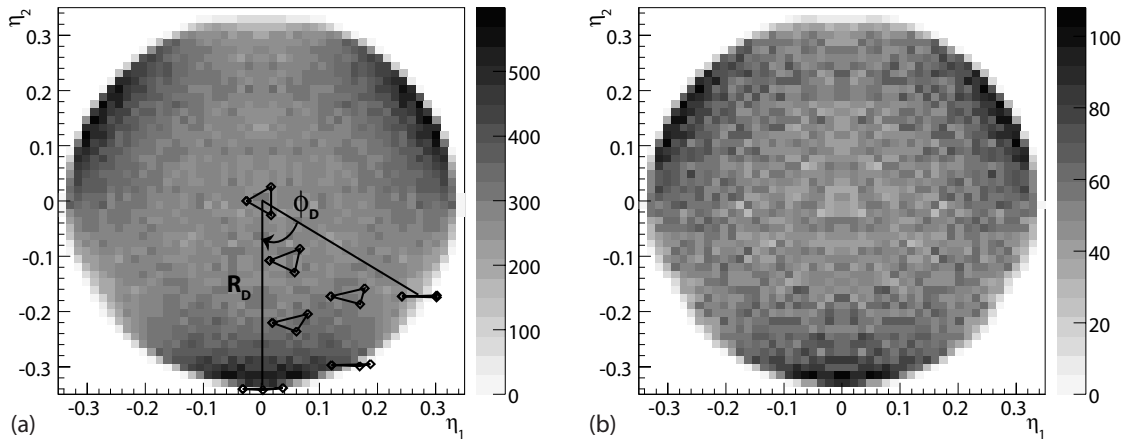


**Figure 6.** The 3D imaging data of hot  $H_3^+$  from the Penning source for a) all dissociations and b) the near-transversal dissociations, i.e., dissociations with  $\cos(\theta) > 0.8$ , where  $\theta$  is the angle between the normal of the molecular plane and the beam axis.

the measured data (not displayed) in order to disregard the anisotropy effects. The hot  $H_3^+$  distribution appears to have a temperature of around 3000 K. For the cold  $H_3^+$ , the least-squares deviation is smallest at the lowest temperature and increases with rising temperature. Although a significant contribution of the  $J=2$  level cannot be excluded, the temperature is most certainly below room temperature, which demonstrates that the ion beams are indeed cold. The apparent difference between experiment and theory at low temperatures can therefore not be explained by considerable heating of the ion beam.

Figure 6a) gives the Dalitz plot of the hot  $H_3^+$  beam from the Penning source for 0-eV collision energy, for the first time acquired by the 3D imaging technique [14]. The geometries of the corresponding dissociations are displayed in the lower sextant. As proof-of-principle for the 3D imaging, the events dissociating near-perpendicular to the detector are displayed in figure 6b). Near-perpendicular events with  $\cos(\theta) > 0.8$  are selected, where  $\theta$  is the angle between the normal of the molecular plane and the beam axis. The transversal 3D Dalitz plot is indeed similar to the total 3D Dalitz plot. The 3D imaging data are also consistent with the Dalitz plots obtained previously by Monte-Carlo reconstructions of 2D projected distance distributions [20].

To investigate the distributions for the different  $H_3^+$  populations in more detail, the Dalitz coordinates have been transformed to polar coordinates (as illustrated in figure 6a) to be able to integrate over the angle and the radius. The integrated radius describes the amount of (non-)linearity and the integrated angle the deformation from the isosceles/equilateral triangle. Figures 7a) and b) display the integrated-coordinate distributions at 0 eV. A uniform background, i.e., isotropic distributed geometries, can be observed superimposed with  $\sim 12\%$  anisotropic dissociations, which exhibit a preference towards linear breakup, independent of the  $H_3^+$  population. As discernable in the Dalitz plot, the near-linear dissociations peak around the symmetric linear breakup and drop to (even slightly below) the level of the isotropic background for the asymmetric linear geometries. The integrated-coordinate distributions show no significant internal-state dependence. Figures 7c) and d) display the distributions for the hot and the cold  $H_3^+$  at 6 meV together with the 0-eV distributions of the hot  $H_3^+$  for comparison. The breakup of

the cold  $H_3^+$  produced with para- $H_2$  at 6 meV was not measured. The fragmentation dynamics of the hot  $H_3^+$  at 6 meV resemble those at 0 eV. The cold  $H_3^+$  breakup exhibits a small difference, peaking slightly more around the symmetric linear dissociations. No large energy dependence is observed.

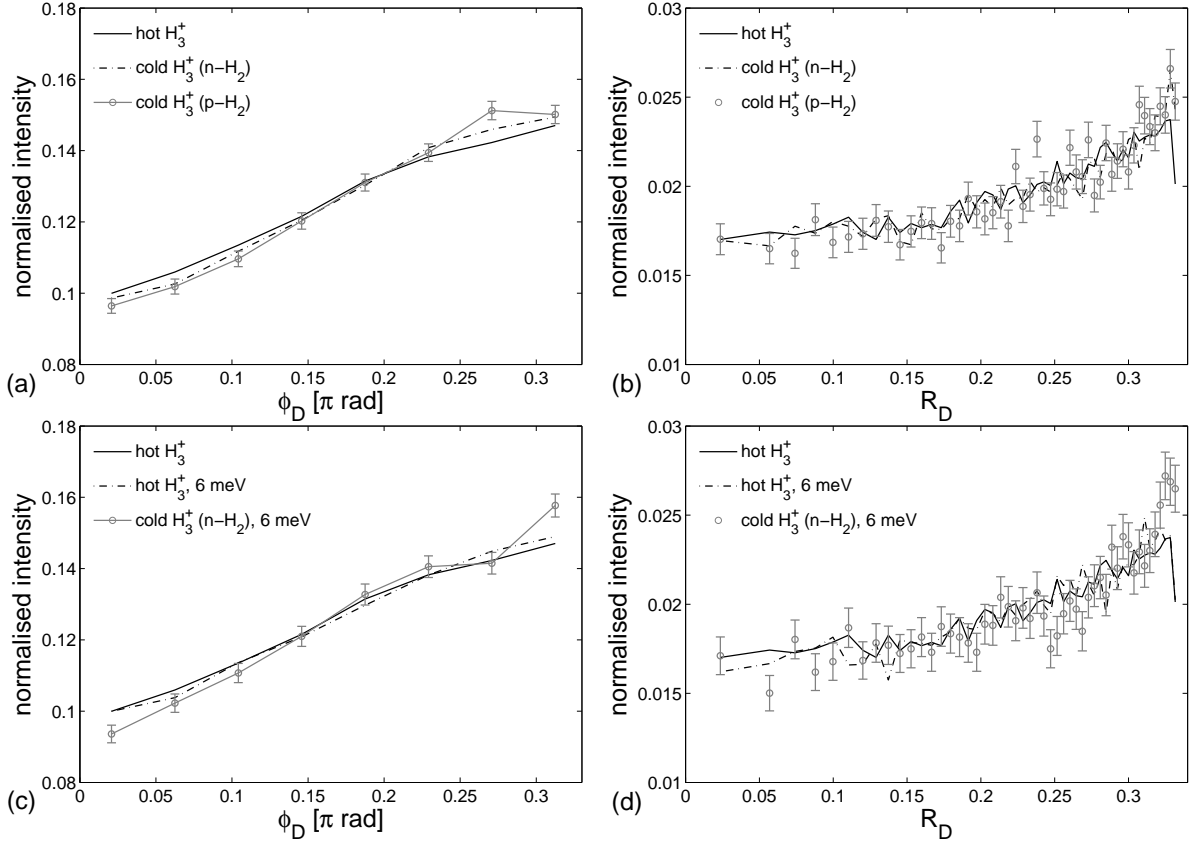


**Figure 7.** The projected Dalitz polar coordinates at a,b) 0 eV and c,d) 6 meV for the given  $H_3^+$  populations. For comparison, the hot  $H_3^+$  data at 0 eV are displayed again with the 6 meV distributions. As illustrated in figure 6,  $R_D$  ranges from the equilateral triangle to linear dissociation geometries and  $\phi_D$  ranges from asymmetric to symmetric geometries. To improve clarity, only the errorbars of the distribution with the lowest statistics are shown.

#### 4. Conclusions

The rovibrational spectroscopy shows that the use of para- $H_2$  as parent gas can indeed enrich the para contribution of the  $H_3^+$  population. In the storage-ring experiment, where the para enrichment cannot be confirmed, no increase in the DR rate has been found when using para- $H_2$  as source gas that may support the prediction of a 10 times higher para- $H_3^+$  rate than ortho- $H_3^+$  rate. The trend of increasing overall rate with increasing temperature as predicted by theory is, however, confirmed by the present data. Furthermore, the  $H_3^+$  ions prepared in the 22-pole trap and transferred to the TSR are really rovibrationally cold, featuring a temperature that is distinctly lower than 300 K. As such, heating effects cannot account for the discrepancy in intensity between the theoretical and experimental rate-coefficient curves. The 3-body fragmentation dynamics of the DR of  $H_3^+$  show no large dependences on the internal-state distribution of the initial  $H_3^+$  nor on electron energy. A fraction of 12% of the  $H_3^+$  ions are

found to dissociate in symmetric near-linear geometries, while 88% have a uniform distribution of geometries.

## Acknowledgments

HB acknowledges partial support from the German Israeli Foundation for Scientific Research and Development (G.I.F.) under Grant I-900-231.7/2005 and by the European Project ITS LEIF (HRPI-CT-2005-026015). We are grateful to the TSR accelerator group for their support during the experiments.

## References

- [1] McCall B J 2005 *Astrochemistry: Recent Successes and Current Challenges Proceedings IAU Symp. No. 231* ed Lis D C, Blake G A and Herbst E pp 165–174
- [2] Oka T 2006 *PNAS* **103** 12235–12242
- [3] Larsson M 2000 *Phil. Trans. R. Soc. Lond. A* **358** 2433–2444
- [4] McCall B J 2006 *Phil. Trans. R. Soc. Lond. A* **364** 2953–2963
- [5] Wolf A, Kreckel H, Lammich L, Strasser D, Mikosch J, Glosik J, Plašil R, Altevogt S, Andrianarijaona V, Buhr H, Hoffmann J, Lestinsky M, Nevo I, Novotny S, Orlov D A, Pedersen H B, Terekhov A S, Toker J, Wester R, Gerlich D, Schwalm D and Zajfman D 2006 *Phil. Trans. R. Soc. Lond. A* **364** 2981–2997
- [6] Greene C H and Kokoouline V 2006 *Phil. Trans. R. Soc. Lond. A* **364** 2965–2980
- [7] Oka T 2000 *Dissociative Recombination: Theory, Experiment and Applications IV* ed Larsson M, Mitchell J B A and Schneider I F (Singapore: World Scientific) pp 13–24
- [8] McCall B J, Huneycutt A J, Saykally R J, Djuric N, Dunn G H, Semaniak J, Novotny O, Al-Khalili A, Ehlerding A, Hellberg F, Kalhori S, Neau A, Thomas R D, Paal A, Österdahl F and Larsson M 2004 *Phys. Rev. A* **70** 052716
- [9] Kreckel H, Motsch M, Mikosch J, Glosik J, Plašil R, Altevogt S, Andrianarijaona V, Buhr H, Hoffmann J, Lammich L, Lestinsky M, Nevo I, Novotny S, Orlov D A, Pedersen H B, Sprenger F, Terekhov A S, Toker J, Wester R, Gerlich D, Schwalm D, Wolf A and Zajfman D 2005 *Phys. Rev. Lett.* **95** 263201
- [10] Glosik J, Korolov I, Plašil R, Novotny O, Kotrik T, Hlavenka P, Varju J, Greene C H, Kokoouline V and Mikhailov I A 2007 (*Preprint arXiv/0710.2339*)
- [11] Kokoouline V and Greene C H 2003 *Phys. Rev. A* **68** 012703
- [12] dos Santos S F, Kokoouline V and Greene C H 2007 *J. Chem. Phys.* **127** 124309
- [13] Kokoouline V and Greene C H 2005 *Phys. Rev. A* **72** 022712
- [14] Strasser D, Urbain X, Pedersen H B, Altstein N, Heber O, Wester R, Bhushan K G and Zajfman D 2000 *Rev. Sci. Instrum.* **71** 3092–3098
- [15] Teloy E and Gerlich D 1974 *Chem. Phys.* **4** 417–427
- [16] Gerlich D 1995 *Phys. Scr.* **T59** 256–263
- [17] Mikosch J, Kreckel H, Wester R, Plašil R, Glosik J, Gerlich D, Schwalm D and Wolf A 2004 *J. Chem. Phys.* **121** 11030
- [18] Kreckel H, Mikosch J, Wester R, Glosik J, Plašil R, Motsch M, Gerlich D, Schwalm D, Zajfman D and Wolf A 2005 *Dissociative Recombination: Theory, Experiment and Applications VI* ed Wolf A, Lammich L and Schmelcher P (London: Institute of Physics and IOP Publishing) pp 126–133
- [19] Orlov D A, Weigel U, Schwalm D, Terekhov A S and Wolf A 2004 *Nuclear instruments and methods in Physics Research A* **532** 418–421
- [20] Strasser D, Lammich L, Kreckel H, Krohn S, Lange M, Naaman A, Schwalm D, Wolf A and Zajfman D 2002 *Phys. Rev. A* **66** 032719
- [21] Nevo I, Novotny S, Buhr H, Andrianarijaona V, Altevogt S, Heber O, Hoffmann J, Kreckel H, Lammich L, Lestinsky M, Pedersen H B, Schwalm D, Wolf A and Zajfman D 2007 *Phys. Rev. A* **76** 022713
- [22] Kreckel H 2003 *Internal excitations of stored triatomic hydrogen molecular ions* Ph.D. thesis University Heidelberg
- [23] Bianca M Dinelli S M and Tennyson J 1992 *J. Mol. Spectrosc.* **153** 718–725